

Improving stability of the metal-free primary energetic cyanuric triazide (CTA) through
cocrystallization

Electronic Supporting Information

Leila M. Foroughi, Ren A. Wiscons, Derek R. Du Bois, Adam J. Matzger*

Department of Chemistry, Macromolecular Science and Engineering Program, University of Michigan,
930 North University Avenue, Ann Arbor, Michigan 48109-1055, United States

Table of Contents

SI 1. Experimental
SI 2. Raman Spectroscopy of 2:1 CTA/BTF, CTA, and BTF
SI 3. Powder X-ray Diffraction of 2:1 CTA/BTF, CTA, and BTF
SI 4. ORTEP Diagrams of 2:1 CTA/BTF, CTA, and BTF
SI 5. Differential Scanning Calorimetry of 2:1 CTA/BTF, CTA, and BTF
SI 6. Thermogravimetric Analysis of 2:1 CTA/BTF, CTA, and BTF
SI 7. Volatility experiments of 2:1 CTA/BTF, CTA, and BTF
SI 8. Morphology of 2:1 CTA/BTF, CTA, and BTF
SI 9. References

SI 1. Experimental

Warning: Although no unplanned detonations were encountered during this work, CTA and BTF are dangerous energetics and CTA has been previously reported to spontaneously explode. Proper safety practices and equipment were used to prevent an explosion due to friction, heat, static shock, impact, and flame. Be aware that the potential for severe injury exists if these materials are handled improperly.

Benzotrifuroxan (BTF) was used as received from Lawrence Livermore National Laboratory. Cyanuric chloride, 99% purity, was purchased from Sigma Aldrich and sodium azide, 99% purity, was purchased from Acros Organics. All reagents were used as received.

Synthesis of cyanuric triazide (CTA)

The synthesis of cyanuric triazide was adapted from the reported procedure.¹ Solutions of cyanuric chloride (414 mg, 2.25 mmol) dissolved in acetone (4.5 mL) and sodium azide (468 mg, 7.20 mmol) dissolved in water (4.5 mL) were stirred together at 30 °C. A white precipitate formed, and after 2 h, the mixture was diluted with water. The crude product was extracted with ethyl acetate (3 × 15 mL), and the organic layers were combined and dried over anhydrous sodium sulfate. The solution of CTA in ethyl acetate was portioned into 10 vials (1 dram) for storage. The dry product is obtained by evaporation of ethyl acetate, yielding a white solid (~363 mg, 79.0% yield), immediately before use. ¹³C NMR (125 MHz, DMSO-*d*₆, δ): 171.53 ppm.

Crystallization

The CTA/BTF cocrystal can be obtained from solvent mediated transformation in a 50/50 by volume isooctane/toluene slurry or from melting CTA in the presence of BTF.

2:1 CTA/BTF from Slurry

CTA (in ethyl acetate) was added to a 4 mL vial and upon evaporation of the solvent, was immediately wetted with a minimal amount of 50/50 by volume isooctane/toluene solution (~100 microliters per 15 mg). An equimolar amount of BTF was added and the vial was placed on a shaker (at RT). After a few hours the crystals were harvested using a vacuum filtration assembly fitted with a disposable 0.45 μm PTFE membrane and washed with cold hexanes. The scale used for the cocrystallization varied between 1-25 mg of CTA. Crystals obtained using this method were subject to single crystal x-ray diffraction and led to the low temperature structure described in the text. Crystals obtained from slurry were used for all characterization (including Raman, TGA, DSC, PXRD, and impact sensitivity) except for the room temperature crystal structure of the cocrystal (crystals obtained from melt; slurry grown crystals yield the same room temperature structure).

2:1 CTA/BTF from Melt

An equimolar quantity of solid CTA and BTF were sealed in a Tzero™ hermetic aluminum DSC pan and heated from 25 to 120 °C (120 °C is above the m.p. of CTA and below of the m.p. of BTF) under a nitrogen purge of 50 mL/min at a heating rate of 5 °C/min. Upon cooling to room temperature, the pan was opened and single crystals were identified and these crystals were characterized by single crystal X-

ray diffraction. The RT crystal structure of the CTA/BTF cocrystal was obtained from a crystal grown with this method. All other DSC experiments are described below.

Raman Spectroscopy

Raman spectra were collected using a Renishaw inVia Raman Spectrophotometer equipped with a Leica microscope, 785 nm lasers, 1200 lines/mm grating, 65 μm slit size and a RenCam CCD detector. Spectra were collected in extended scan mode from 100-3600 cm^{-1} and analyzed using the WiRE 3.4 software package (Renishaw). Variable temperature Raman spectra were collected by placing a few crystals on a Linkam LTS 350 heating stage which was connected to the Raman system described above. The samples were heated from room temperature to ~ 10 $^{\circ}\text{C}$ above melt for each compound (CTA 105 $^{\circ}\text{C}$, CTA/BTF 155 $^{\circ}\text{C}$, and BTF 205 $^{\circ}\text{C}$) at a rate of 5 $^{\circ}\text{C}/\text{min}$. Spectra were collected every 5 $^{\circ}\text{C}$ in static scan mode centered at 520 cm^{-1} (209-809 cm^{-1}).

Powder X-ray Diffraction

Powder X-ray Diffraction (PXRD) patterns were collected at room temperature using a Rigaku SmartLab X-ray Diffractometer using Cu-K α radiation in point focus mode outfitted with a Pilatus 2D detector. Patterns were collected in continuous mode from 4 to 50 $^{\circ}$ with a step speed of 2.5 degrees per min.

Single-Crystal Structure Determination

Single-crystal X-ray diffraction data were collected using a Rigaku XtaLAB Synergy-S X-ray diffractometer configured in a kappa goniometer geometry. The diffractometer is equipped with a low temperature device and a PhotonJet-S microfocus Cu source ($\lambda = 1.54187$ \AA) operated at 50 kV and 1 mA. X-ray intensities were measured at 100(1) K with the HyPix-6000HE detector placed 34.00 mm from the sample. The data were processed with CrysAlisPro v38.46 (Rigaku Oxford Diffraction) and corrected for absorption (specific details available in the crystallographic information file for each structure). The structures were solved in OLEX2² using SHELXTL³ and refined using SHELXL.⁴ All non-hydrogen atoms were refined anisotropically.

Table S1. Low temperature (100 K) crystallographic data for 2:1 CTA/BTF

Material	CTA/BTF
Space Group	<i>C2/c</i>
<i>a</i> \AA	16.6224(3)
<i>b</i> \AA	11.4096(3)
<i>c</i> \AA	12.9021(3)
α ($^{\circ}$)	90
β ($^{\circ}$)	97.1063(19)
γ ($^{\circ}$)	90
Volume (\AA^3)	2428.15
Temperature (K)	100.0(1)
ρ_{calc} (g cm^{-3})	1.807
R_1/wR_2 (%/%)	2.72/7.21

Table S2. Room temperature crystallographic data for 2:1 CTA/BTF

Material	CTA/BTF
Space Group	<i>C2/c</i>
<i>a</i> Å	17.0625(1)
<i>b</i> Å	11.4704(1)
<i>c</i> Å	13.0200(1)
α (°)	90
β (°)	97.7278
γ (°)	90
Volume (Å ³)	2525.144
Temperature (K)	298.4(4)
ρ_{calc} (g cm ⁻³)	1.737
R_1/wR_2	7.93/26.85
GOF	1.025

Calculations

Spartan 16 was used to calculate the electrostatic potential maps, the energy profile around the C-N3 bond, and geometry optimization. The methods used are listed in Fig. 1.

Table S3. Energy calculations

The below energies were obtained from geometry optimization calculations (MP2/6-31G(d,p)) of C_{3h} , the transition state, and C_s . They were used to calculate the relative energies show in Fig. 1b.

	Hartrees	Kcal mol ⁻¹
C_{3h}	-769.39279	-482800.9009
TS	-769.37421	-482789.2405
C_s	-769.39228	-482800.5796

Sensitivity

Sensitivity to mechanical stimuli:

The impact sensitivity of CTA and the cocrystal were determined using an in-house apparatus.⁵ A 5.246 lb stainless-steel weight was dropped from varying heights onto aluminum DSC pans containing 2 mg \pm 10%. Over 40 samples of each material were tested and the Dh_{50} was measured as the drop height at which there was a 50% probability of detonation.

Energetic Performance Calculations

Energetic performance values were predicted using the thermochemical code Cheetah 7.0. The heat of formation for CTA/BTF was obtained by considering the material as a physical mixture of the constituents. The heat of formation for BTF was obtained from the JCZS product library revision 32 and the heat of formation for CTA was obtained from the literature.⁶ Cheetah 7.0 calculations were performed using the Sandia JCZS product library revision 32.

Table S4. Calculated (Cheetah.7.0) performance values

	ρ_{calc} (g cm ⁻³)	Detonation Velocity (km/s)	Detonation Pressure (GPa)
CTA	1.723	8.056	26.366
CTA/BTF	1.737	8.152	27.583
BTF	1.901	8.725	35.146

Differential Scanning Calorimetry

Thermograms of CTA, BTF, and CTA/BTF were recorded on a TA Instruments Q10 DSC. All samples were sealed in TA hermetic aluminum pans with a sample purge flow of nitrogen of 50 mL/min. The samples were heated from room temperature to 400 °C at 5 °C/min. The instrument was calibrated using an indium standard. Thermograms were analyzed using TA Universal Analysis 2000, V 4.5A.

Thermogravimetric Analysis

Thermogravimetric analysis (TGA) thermograms for each sample were recorded on a TA Instruments Q50 TGA. Samples were placed directly on a tared platinum pan and were heated at 5 °C/min. CTA and the cocrystal were heated to 250 °C and BTF was heated to 400 °C. The nitrogen purge flow over the samples was 60 mL/min and the purge flow for the balance was 40 mL/min. The instrument was calibrated using the Curie points of alumel and nickel standards. The thermograms were analyzed using TA Universal Analysis 2000, V 4.5.

Vapor Pressure Measurements

The relative volatility of CTA and the CTA/BTF cocrystal were determined by the measuring the mass lost as a function of time at three different temperatures. Each sample (~2 mg CTA or CTA/BTF) was sealed in a TA instruments Tzero aluminum pan with a lid that had a hole punched in it using a machined die (area of hole 3.43E-07 m²). Using the TA Instruments Q50 TGA, the pans containing sample were placed on a platinum TGA pan and heated from room temperature to 85, 100, and 115 °C at 20 °C/min and held isothermally. The nitrogen purge flow over the samples was 60 mL/min and the purge flow for the balance was 40 mL/min. The data were plotted as weight (mg) lost over time (min) (Fig. S12 and S13) and the slope provided the rate of weight loss, dm/dt (Table S2). Weight loss at each temperature was expressed relative to the highest rate of loss, CTA at 115 °C (Figure 4). The degree by which volatility was suppressed was calculated by dividing the relative loss of CTA by the relative loss of cocrystal at each temperature (Table S3 and Figure 4).

SI 2. Raman Spectra of 2:1 CTA/BTF, CTA, and BTF

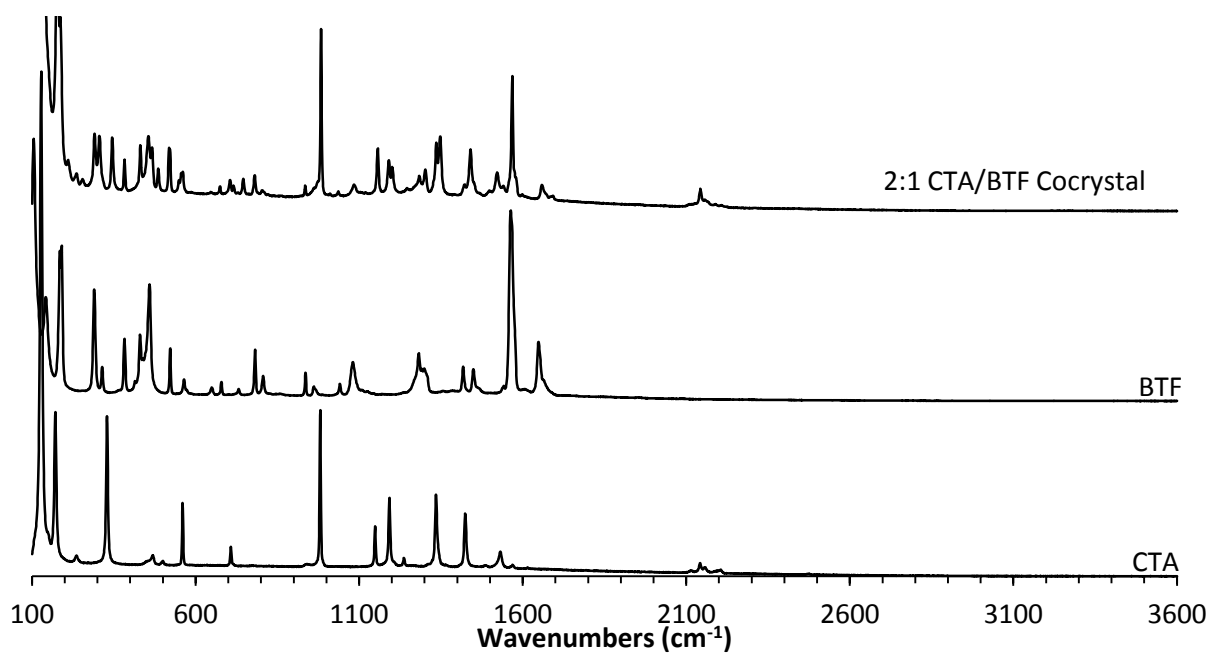


Figure S1. Full Range (100-3600 cm^{-1}). Raman spectra of the 2:1 CTA/BTF cocrystal, BTF, and CTA.

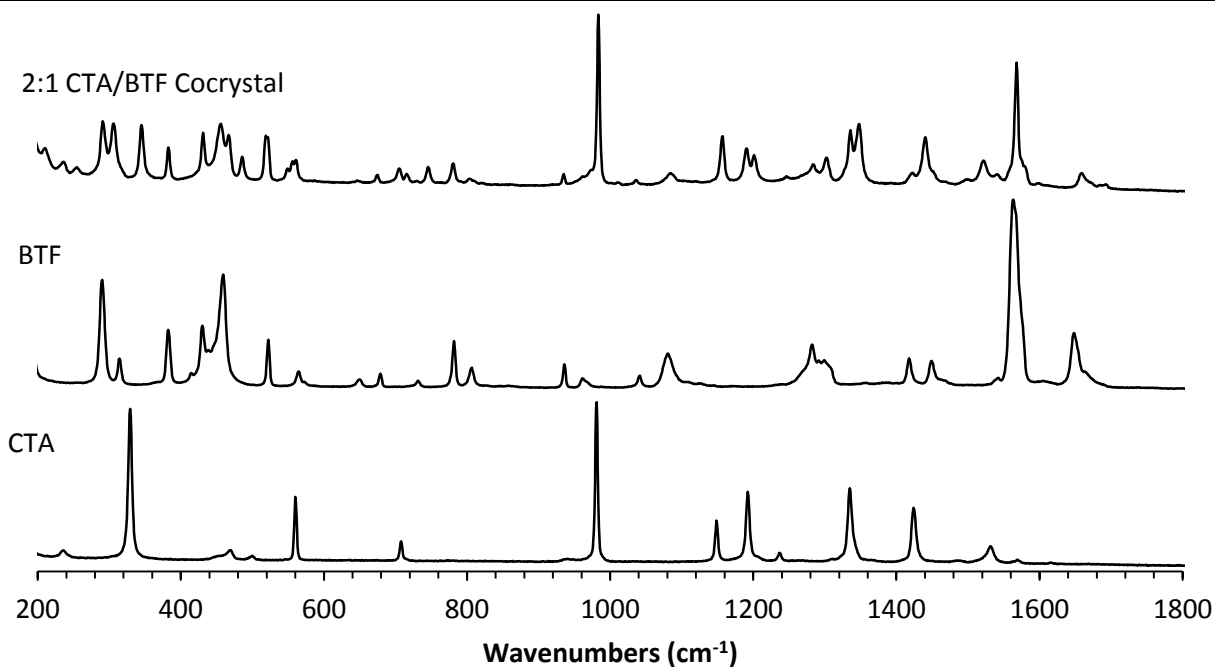


Figure S2. Zoomed in (200-1800 cm^{-1}). Raman spectra of the 2:1 CTA/BTF cocrystal, BTF, and CTA.

SI 3. Powder X-ray Diffraction

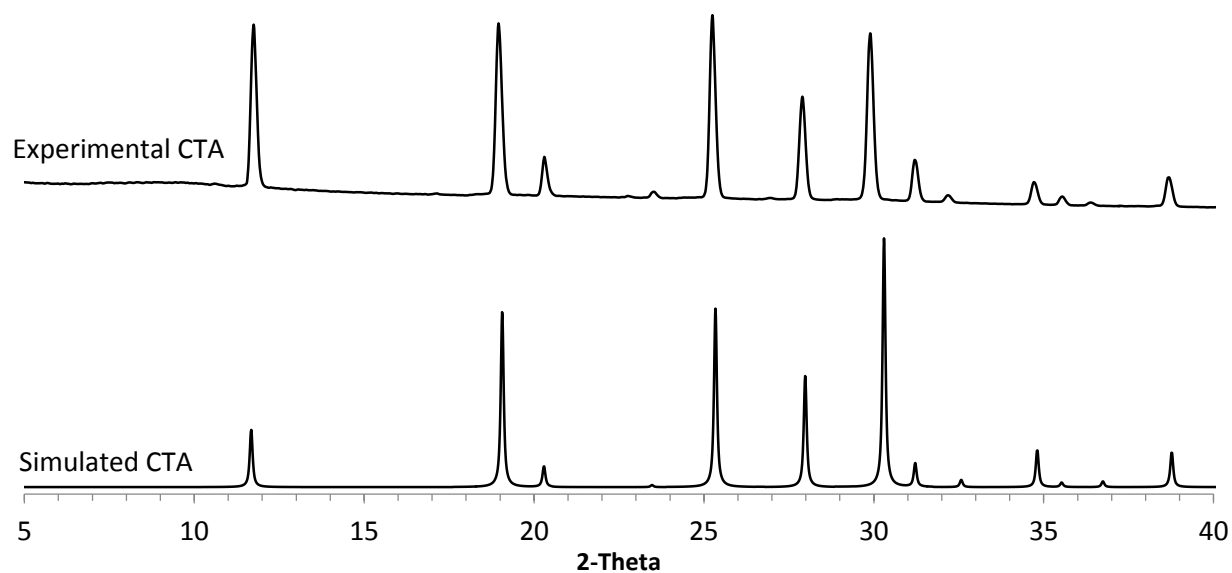


Figure S3. PXRD data for CTA and the simulated powder pattern for CTA from the crystal structure (ref code: CYNURZ01).⁷

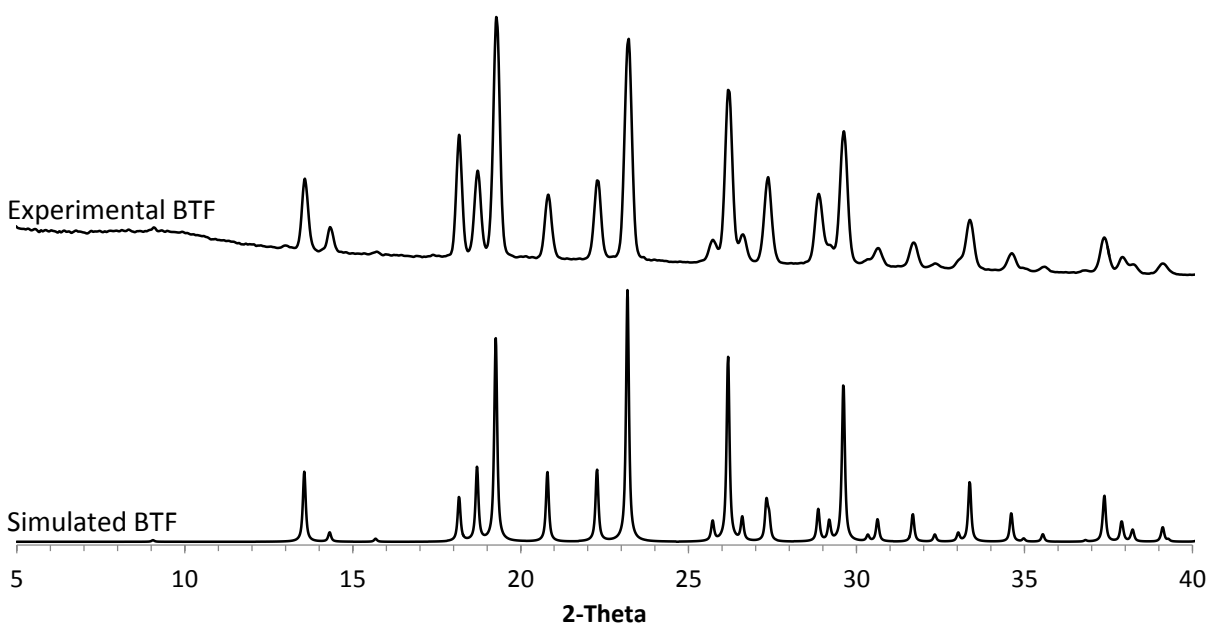


Figure S4. PXRD data for BTF and the simulated powder pattern for BTF from the crystal structure (Ref code: BOXFOX).⁸

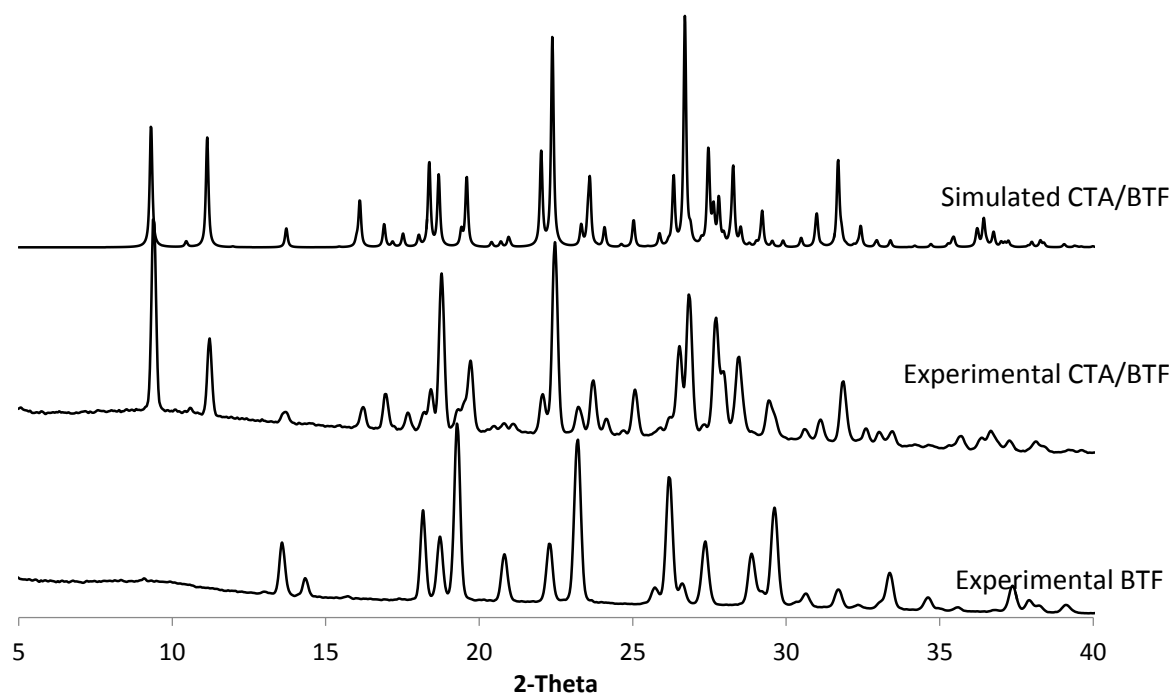


Figure S5. The simulated powder pattern for 2:1 CTA/BTF generated from the room temperature crystal structure, PXRD data for 2:1 CTA/BTF and BTF.

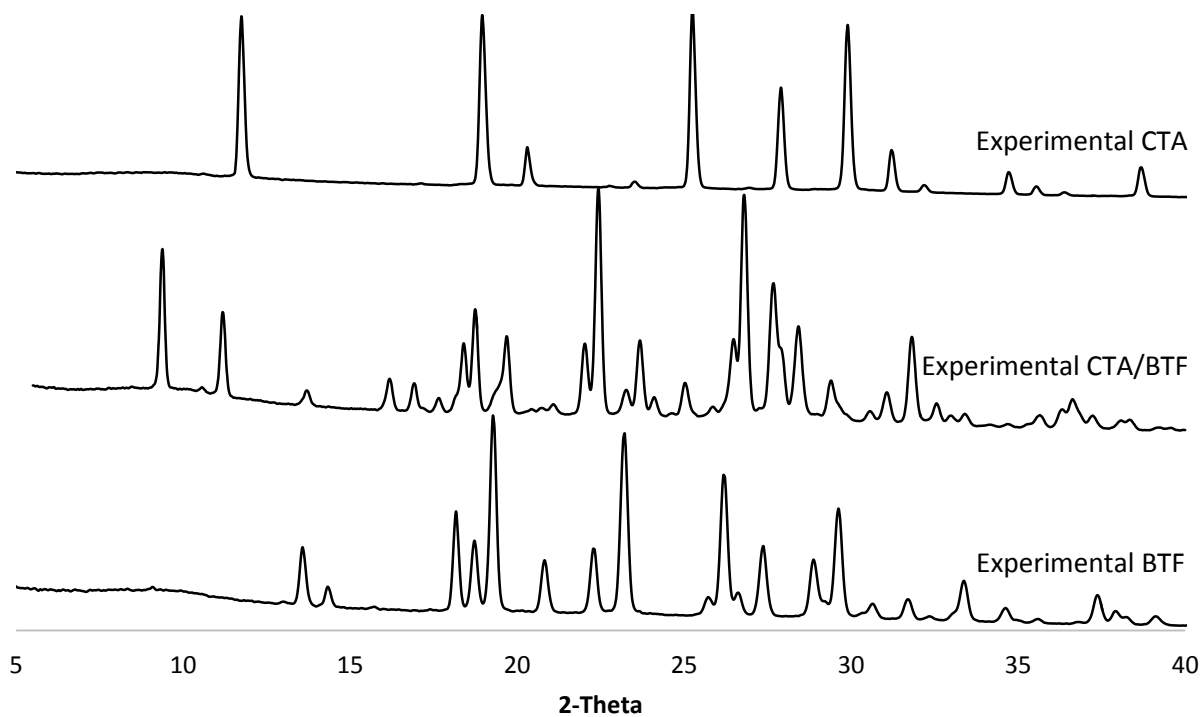


Figure S6. PXRD data for CTA, 2:1 CTA/BTF, and BTF.

SI 4. ORTEP of the 2:1 CTA/BTF Cocrystal

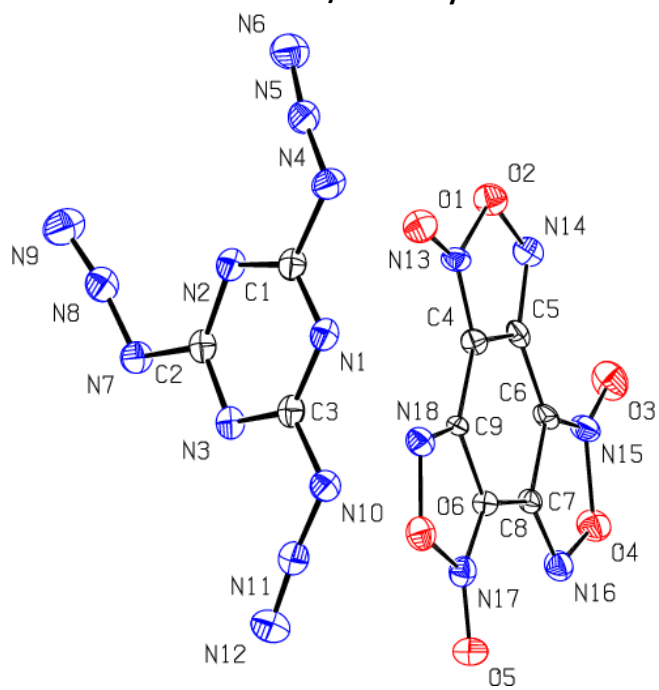


Figure S7. ORTEP diagram for 2:1 CTA/BTF collected at 100 K.

SI 5. Differential Scanning Calorimetry of 2:1 CTA/BTF

Exo Up

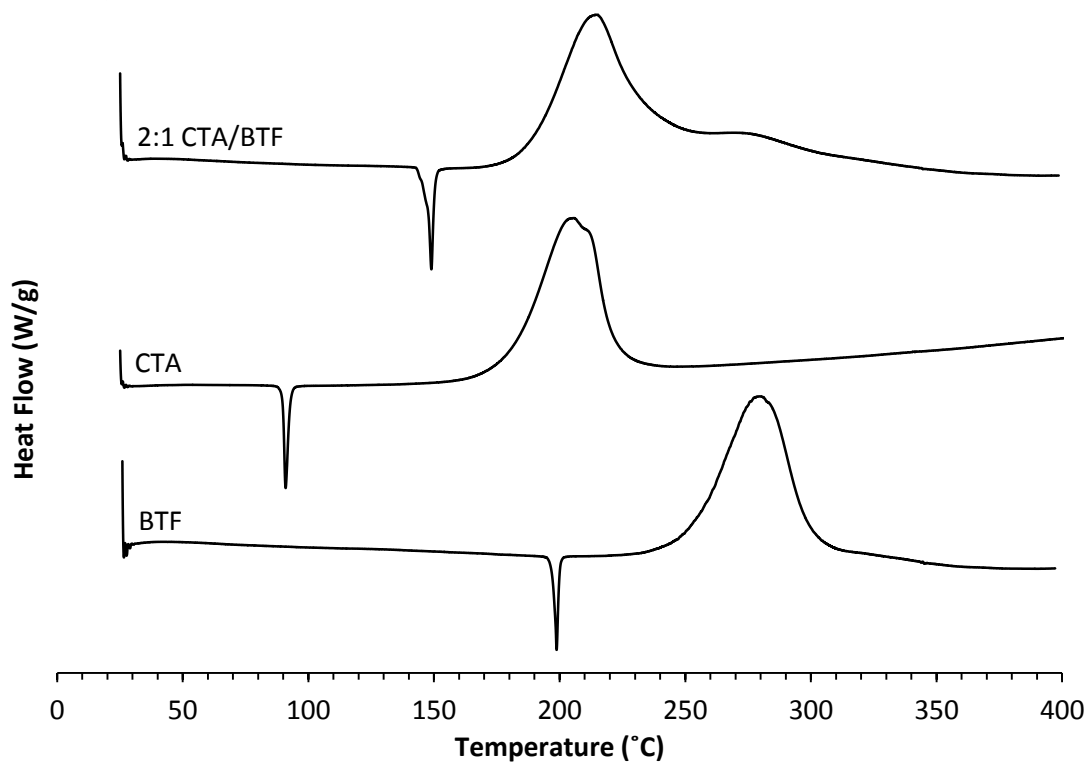


Figure S8. Typical DSC traces of 2:1 CTA/BTF, CTA, and BTF

SI 6. Thermogravimetric Analysis of the 2:1 CTA/BTF , CTA, and BTF

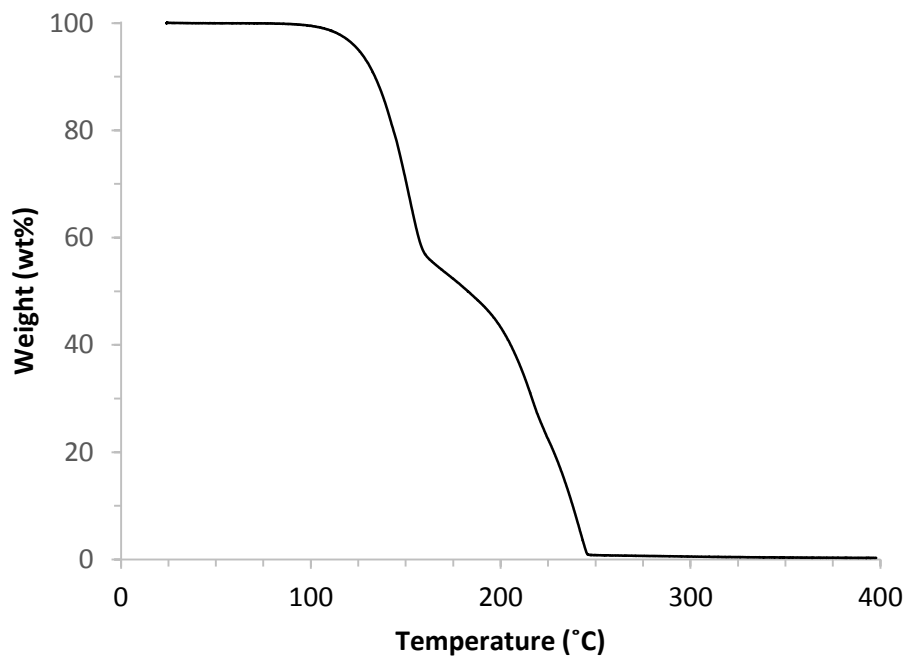


Figure S9. Typical TGA traces of the 2:1 CTA/BTF cocrystal.

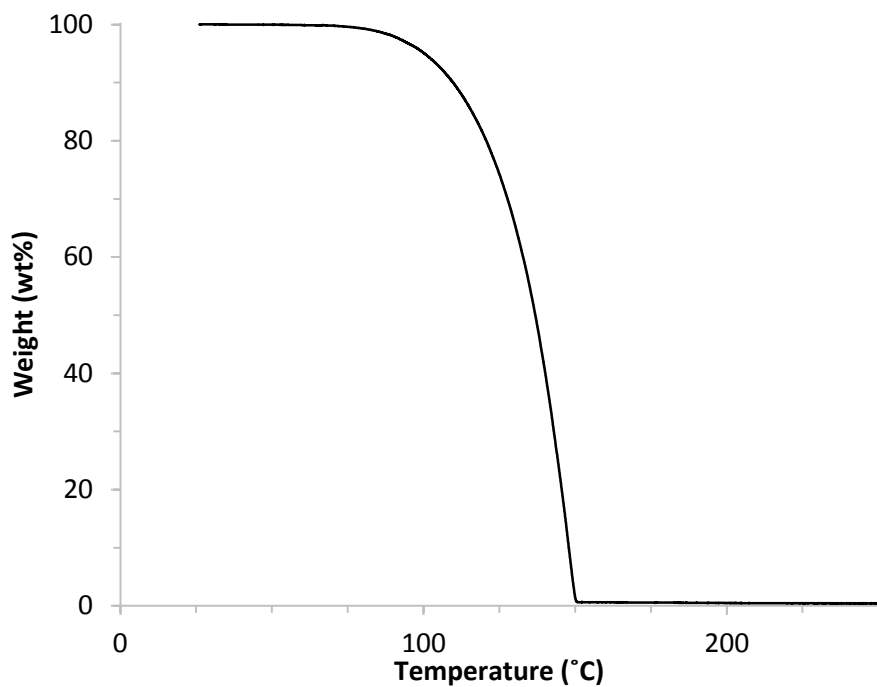


Figure S10. Typical TGA trace of CTA.

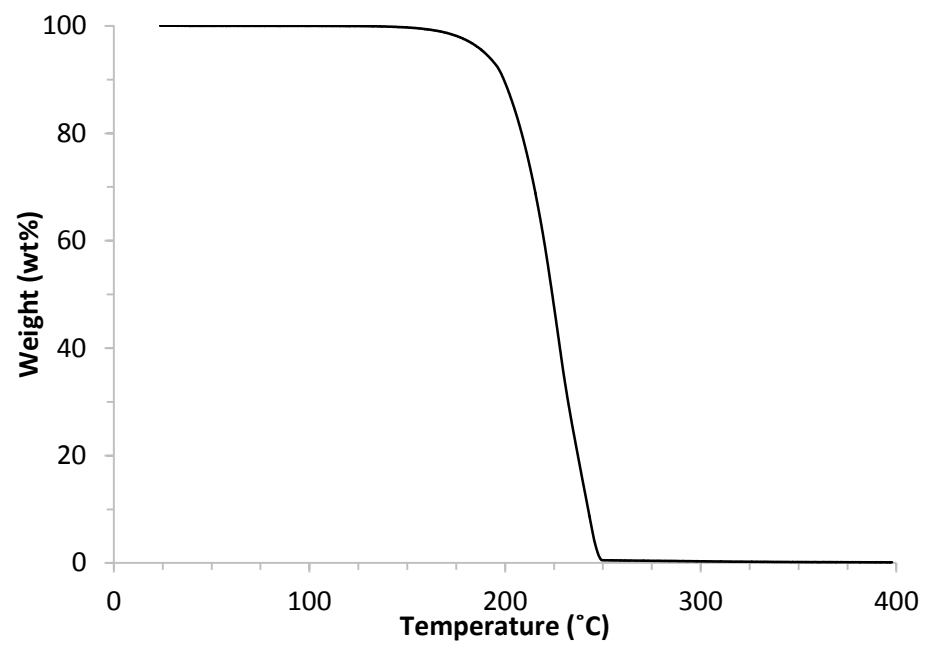


Figure S11. Typical TGA trace of BTF.

SI 7. Measuring Volatility of the 2:1 CTA/BTF Cocrystal and CTA

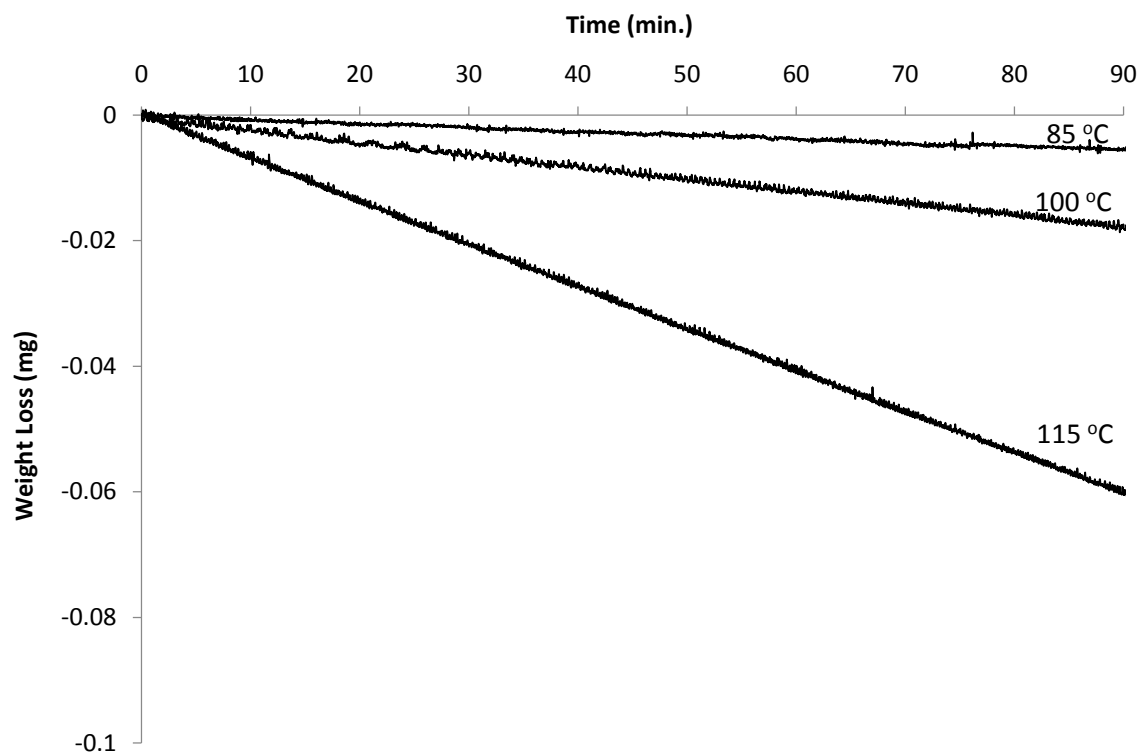


Figure S12. Weight loss of 2:1 CTA/BTF cocrystal as a function of time at 85 °C, 100 °C, and 115 °C.

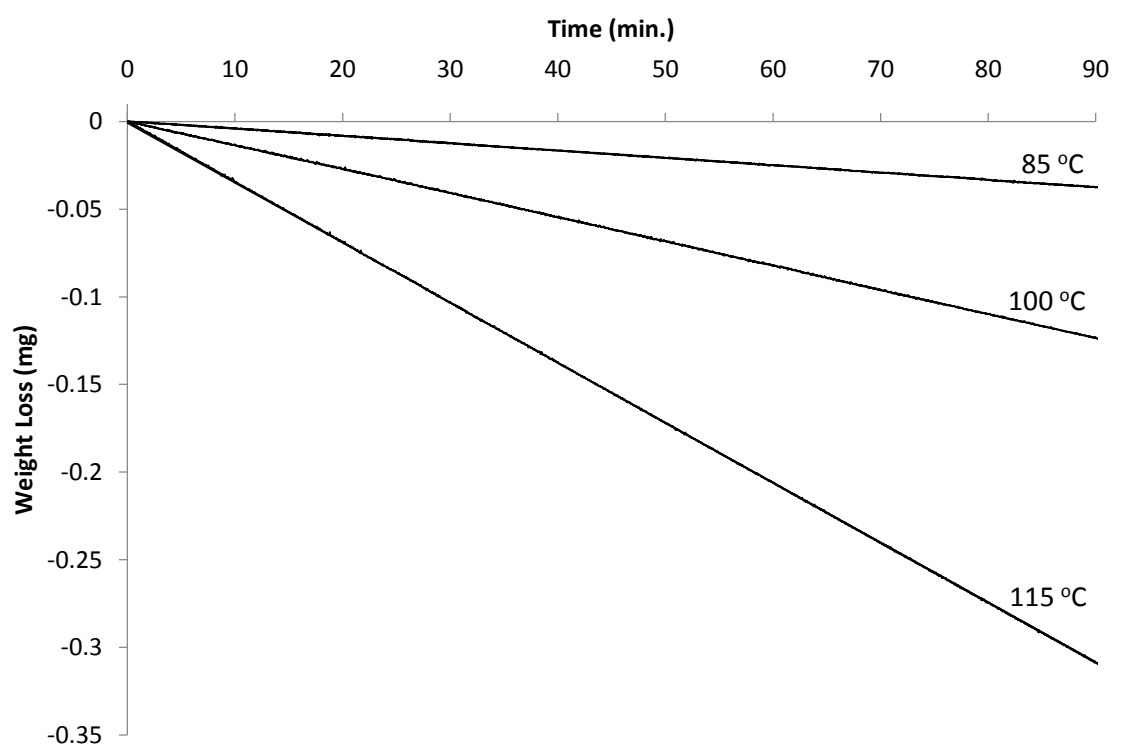


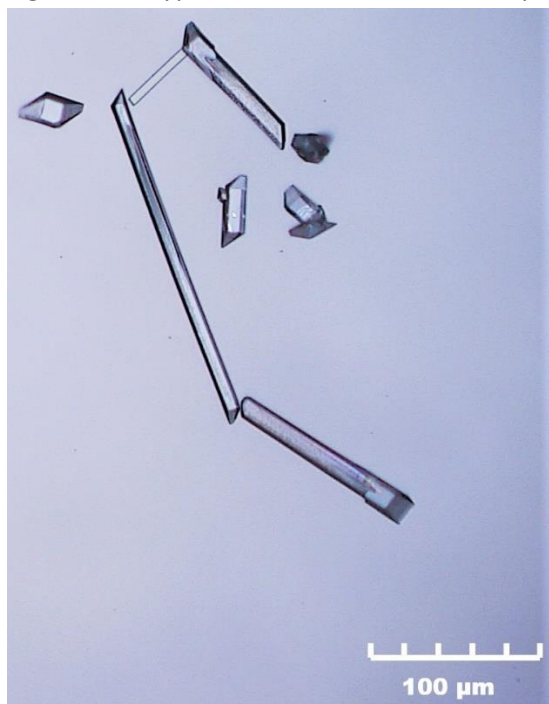
Figure S13. Weight loss of CTA as a function of time at 85 °C, 100 °C, and 115 °C.

Table S5. Dm/dt (slope of fitted line in mg/min) and the degree by which volatility was suppressed (ratio of dm/dt of CTA/(CTA/BTF)).

	85 °C	100 °C	115 °C
CTA/BTF*	0.0000547	0.000192	0.000646
CTA*	0.000413	0.00137	0.00341
$(dm/dt \text{ CTA})/(dm/dt \text{ CTA/BTF})$	7.6	7.1	5.3

S18. Morphology of the 2:1 CTA/BTF Cocrystal

Figure S14. Typical colorless blade-like morphology of the 2:1 CTA/BTF cocrystal grown from slurry.



SI9. References

- 1 X. Chen, Q. Jin, L. Wu, C. Tung and X. Tang, *Angew. Chem. Int. Ed Engl.*, 2014, **53**, 12542–12547.
- 2 O. V. Dolomanov, L. J. Bourhis, R. J. Gildea, J. A. K. Howard and H. Puschmann, *J. Appl. Crystallogr.*, 2009, **42**, 339–341.
- 3 G. M. Sheldrick, *Acta Crystallogr Sect Found Adv*, 2015, **71**, 3–8.
- 4 G. M. Sheldrick, *Acta Crystallogr Sect C Struct Chem*, 2015, **71**, 3–8.
- 5 J. C. Bennion, N. Chowdhury, J. W. Kampf and A. J. Matzger, *Angew Chem Int Ed*, 2016, **128**, 13312–13315.
- 6 E. G. Gillan, *Chem. Mater.*, 2000, **12**, 3906–3912.
- 7 E. Keßnich, T. M. Klapötke, J. Knizek, H. Nöth and A. Schulz, *Eur. J. Inorg. Chem.*, 1998, **1998**, 2013–2016.
- 8 H. H. Cady, A. C. Larson and D. T. Cromer, *Acta Crystallogr.*, 1966, **20**, 336–341.